catalysts

MDPI

Article

Characterization and Catalytic Activity of Mn-Co/TiO_2 Catalysts for NO Oxidation to NO_2 at Low Temperature

Lu Qiu, Yun Wang, Dandan Pang, Feng Ouyang *, Changliang Zhang and Gang Cao

Received: 7 November 2015; Accepted: 5 January 2016; Published: 11 January 2016
Academic Editor: Michalis Konsolakis

Environmental Science and Engineering Research Center, Shenzhen Graduate School, Harbin Institute of Technology, Shenzhen 518055, China; qlu198572@yahoo.com (L.Q.); febmeow@hotmail.com (Y.W.); ddpang12@gmail.com (D.P.); zcl19900617@outlook.com (C.Z.); caog@hotmail.com (G.C.)
* Correspondence: ouyangfh@hit.edu.cn; Tel./Fax: +86-755-260-33472

Abstract: A series of Mn-Co/TiO_2 catalysts were prepared by wet impregnation method and evaluated for the oxidation of NO to NO_2. The effects of Co amounts and calcination temperature on NO oxidation were investigated in detail. The catalytic oxidation ability in the temperature range of 403–473 K was obviously improved by doping cobalt into Mn/TiO_2. These samples were characterized by nitrogen adsorption-desorption, X-ray diffraction (XRD), X-ray photoelectron spectroscopy (XPS), transmission electron microscope (TEM) and hydrogen temperature programmed reduction (H_2-TPR). The results indicated that the formation of dispersed Co_3O_4·$CoMnO_3$ mixed oxides through synergistic interaction between Mn-O and Co-O was directly responsible for the enhanced activities towards NO oxidation at low temperatures. Doping of Co enhanced Mn^{4+} formation and increased chemical adsorbed oxygen amounts, which also accelerated NO oxidation.

Keywords: NO Oxidation; NO_2; mixed oxides; manganese; cobalt; interaction

1. Introduction

Nitrogen oxides (NO_x) in the exhaust from stationary and mobile sources are toxic to human's health and have brought environmental problems, such as photochemical smog, acid rain and ozone depletion. NO_x storage-reduction (NSR) and selective catalytic reduction (SCR) are considered to be promising technologies to achieve high NO_x reduction efficiency. It is known that most nitrogen oxides from exhaust emissions exist in the form of NO (>90%). NO oxidation is considered to be a key step for NO_x reduction on both the NSR and SCR reactions. In the process of NSR, NO is first oxidized to NO_2 and then stored on the basic components of catalysts as nitrates [1]. For SCR, NO_2 is favored for NO_x conversion according to the so-called Fast SCR reaction, which is thought to be faster by one order of magnitude than the Standard SCR reaction under oxidizing conditions [2]. The light-off temperature in the NO oxidation to NO_2 is significant for the low-temperature SCR of NO_x reduction. Therefore the research into NO oxidation catalysts is important for the NO_x removal and various catalysts have been researched, including the supported noble metals [3–6] and other metal oxides [7–9].

Among these catalysts, there has been some attention focused on cobalt oxides [10] and manganese oxides [11]. It was reported that cobalt oxides possess better oxidation ability [12–14]. Co^{2+}/Co^{3+} oxidation states were found to interconvert readily in oxidizing and reducing conditions [15]. The presence of Co_3O_4 means high activity for oxidation reactions [10,16]. In addition, Mn-based catalysts have been proven to be highly active for the low-temperature SCR reaction, which would avoid the disadvantages associated with the commercial high-temperature catalysts. Several manganese based catalysts, such as the Mn/TiO_2 [17,18] and the Mn catalysts doped with other metal (Fe, Co, Ni, Cu,

Ce, *etc.*) oxides [19–21], have been reported for the low-temperature SCR reaction. As reported in the literature [22,23], Mn oxides not only acted as highly efficient SCR catalysts, but also showed certain catalytic activity for NO oxidation. The Mn-Co/TiO_2 catalysts have been evaluated for the low temperature SCR reaction [19]. However, the activities of Mn-Co/TiO_2 for NO oxidation to NO_2 have been reported rarely.

The present work aims to investigate the catalysts of Mn-Co composite oxides loaded on TiO_2 for NO oxidation at low temperatures. The catalysts with different Co contents and calcined at different temperatures were investigated to determine the interactions between cobalt oxides and manganese oxides. Special attention was paid to the Mn-O-Co mixed oxides which can change the properties of the catalysts and enhance the oxidation ability. The Mn-Co/TiO_2 catalysts were characterized by means of N_2 adsorption-desorption, X-ray diffraction (XRD), transmission electron microscopy (TEM), X-ray photoelectron spectroscopy (XPS) and hydrogen temperature-programmed reduction (H_2-TPR).

2. Results and Discussion

2.1. Activity of NO Oxidation to NO_2

Figure 1 shows the oxidation efficiency of NO to NO_2 over a series of Mn-Co/TiO_2 catalysts with different cobalt contents and a constant loading of 10 wt. % manganese. These catalysts were calcined at 773 K. As a reference, the activities of 10Co/TiO_2, 10Mn/TiO_2 and 20Mn/TiO_2 were also tested. As shown in Figure 1, the NO conversion efficiencies of 10Mn/TiO_2 and 20Mn/TiO_2 were higher than that of 10Co/TiO_2 below 513 K. Dramatic increase in the NO oxidation ratio within the temperature range of 403–473 K was observed upon addition of cobalt oxides to Mn/TiO_2. However, the NO conversion increased slowly with increasing Co content above 473 K. The 10Mn-10Co/TiO_2 exhibited a maximum oxidation efficiency of 61% at 543 K, which was nearly equal to that of 10Co/TiO_2. The activity results implied that strong interactions might exist between Co and Mn oxides, which could promote the NO oxidation to NO_2 at low temperatures.

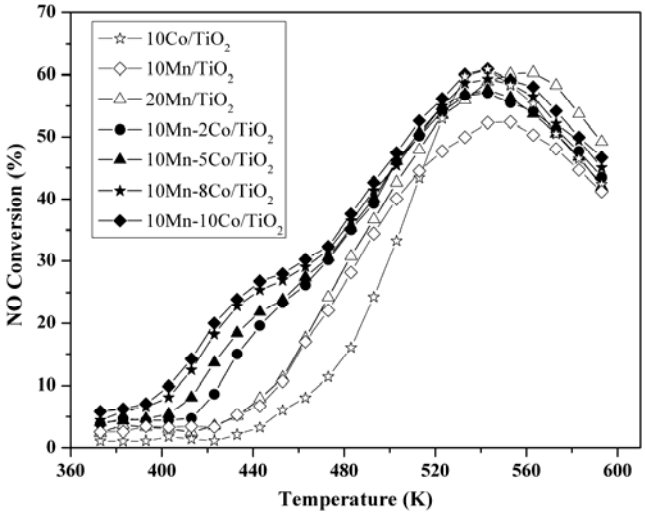

Figure 1. NO oxidation efficiency of Mn-Co/TiO_2 catalysts with different Co contents. Reaction conditions: [NO] = 400 ppm, [O_2] = 5%, Ar balance, GHSV = 42,000 h^{-1}.

Figure 2 shows the oxidation efficiency of NO to NO_2 over a series of 10Mn-5Co/TiO_2 catalysts calcined at various temperatures. It can be seen that the catalytic activity increased with the calcination temperature increase from 573 to 773 K, and then decreased. The catalyst Mn-Co/TiO_2 (773 K) had the highest oxidation efficiency at 543 K among these samples. However, the Mn-Co/TiO_2 calcined at 573 and 673 K exhibited excellent catalytic activities in the temperature range of 403–483 K.

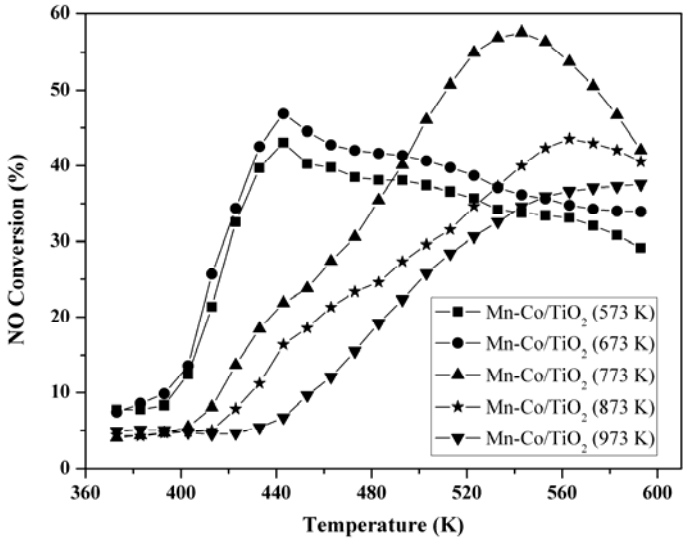

Figure 2. NO oxidation efficiency of 10Mn-5Co/TiO_2 catalysts calcined at different temperatures. Reaction conditions: [NO] = 400 ppm, [O_2] = 5%, Ar balance, GHSV = 42,000 h^{-1}.

2.2. Nitrogen Adsorption-Desorption Characterization

The specific surface areas and pore volumes for Mn-Co/TiO_2 catalysts were determined by nitrogen adsorption-desorption method. The results are listed in Table 1. A consistently decreasing trend of surface areas with increasing calcination temperature was noted for 10Mn-5Co/TiO_2 samples, and a little decrease with the increased Co contents was also showed.

Table 1. BET surface areas and average pore diameters of Mn-Co/TiO_2 catalysts with various Co contents and calcined at different temperatures.

Catalyst	S_{BET} ($cm^2 \cdot g^{-1}$)	Average Pore Diameter (nm)
10Mn/TiO_2 (773 K)	48.35	8.67
10Mn-5Co/TiO_2 (573 K)	50.57	7.21
10Mn-5Co/TiO_2 (673 K)	50.38	6.86
10Mn-5Co/TiO_2 (773 K)	45.79	8.52
10Mn-5Co/TiO_2 (873 K)	30.51	8.38
10Mn-5Co/TiO_2 (973 K)	7.01	6.27
10Mn-10Co/TiO_2 (773 K)	42.13	8.02

2.3. XRD Characterization

Figure 3 shows the X-ray powder diffraction patterns of the Mn-Co/TiO_2 catalysts calcined at 773 K, with different Co contents ranged from 0 to 10 wt. %. It can be seen that the relative strong patterns showed diffraction peaks corresponding to anatase TiO_2 phase (PDF#21-1272) and rutile phase (PDF#21-1276), while anatase was the main form in these catalysts. In the pattern of 10Co/TiO_2 (Figure 3a), several weak diffraction peaks were detected at 2θ values of 18.8°, 31.2°, 44.7°, 59.3° and 65.2°, corresponding to Co_3O_4 phase (PDF#43-1003). In the pattern of 10Mn/TiO_2 (Figure 3b), these weak peaks at 2θ values of 37.3° and 42.7° can be attributed to MnO_2 (PDF#50-0866). However, the crystalline MnO_2 was poor since its corresponding diffraction peaks were very weak.

For the Mn-Co/TiO_2 samples with different Co contents, several weak peaks appeared at 18.4°, 30.8°, 33.4°, 44.1°, 58.9° and 65.5° (Figure 3d–g). The intensities of these peaks were enhanced slightly by the increase of Co contents. Compared with the pattern of 10Co/TiO_2, these peaks had a slight shift toward lower or higher 2θ value. These peaks at 30.8°, 33.4°, 58.9° and 65.5° can be assigned to $CoMnO_3$, while the peaks at 18.4° and 44.1° were ascribed to $CoMn_2O_4$. These peaks were also

weak, inferring that most of the binary metal oxides existed in highly dispersed state. However, the intensities of these peaks were enhanced when the content of Mn increased to 20 wt. % and the Co content was 10 wt. % (Figure 3g). The existence of $CoMnO_3$ and $CoMn_2O_4$ was also demonstrated by Meng *et al.* [24] when Co oxides and Mn oxides were mixed without the support TiO_2. It can be deduced that $CoMnO_3$ and $CoMn_2O_4$ were two types of Mn-Co composite oxides formed on surface of TiO_2, in which Mn ions existed mainly in valence states of Mn^{4+} and Mn^{3+}, respectively.

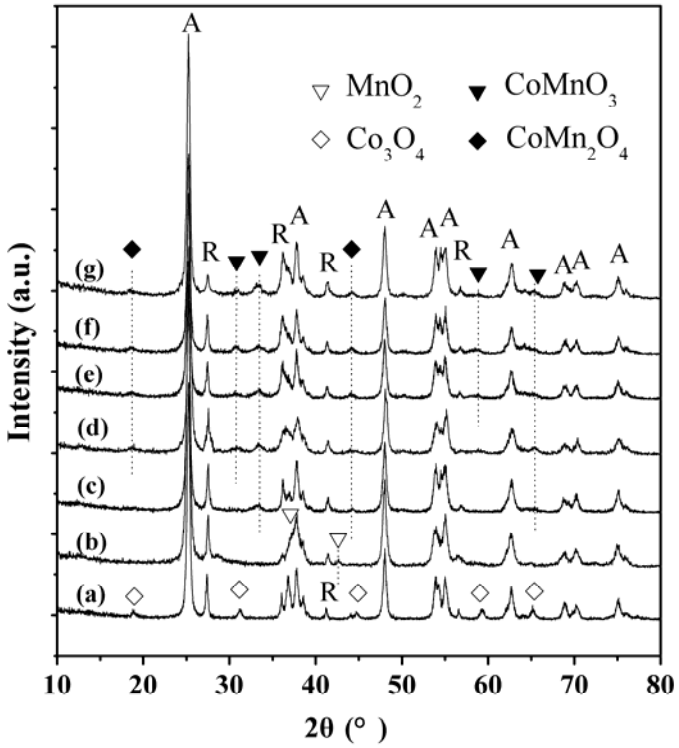

Figure 3. XRD patterns of the catalysts Mn-Co/TiO_2 (773 K) with different Co contents: (**a**) 10Co/TiO_2; (**b**) 10Mn/TiO_2; (**c**) 10Mn-2Co/TiO_2; (**d**) 10Mn-5Co/TiO_2; (**e**) 10Mn-8Co/TiO_2; (**f**) 10Mn-10Co/TiO_2; and (**g**) 20Mn-10Co/TiO_2. (A = anatase phase of TiO_2, R = rutile phase of TiO_2).

Figure 4 shows the XRD patterns of 10Mn-5Co/TiO_2 catalysts calcined at various temperatures. It can be seen that the intensities of rutile TiO_2 peaks were enhanced with calcination temperature increasing while the intensities of anatase peaks were decreased, indicating the transformation of anatase to rutile. The samples calcined at 573 and 673 K were low crystallized with the Mn-O-Co mixed oxides (Figure 4a,b). The weak crystal structure of $CoMnO_3$ and $CoMn_2O_4$ were only detected until the calcination temperature reached 773 K, represented by the peaks at 18.4°, 30.8°, 33.4°, 44.1° and 65.5°. These peaks decreased or disappeared above 873 K. Evidently, NO oxidation efficiency is related to the dispersion of $CoMnO_3$ and the crystal types of TiO_2.

As the calcination temperature increased to 873 and 973 K, the peaks at 18.4°, 30.8° and 33.4° shifted slightly toward lower 2θ value. We considered that was due to the transformation of Mn^{4+} to Mn^{3+} and Mn^{3+} to Mn^{2+} in the process of sintering. The peak at 32.9° can be attributed to $CoMn_2O_4$ phase and the peaks appeared at 18.1°, 29.2° and 60.6° can be attributed to a more complex $(Co,Mn)(Co,Mn)_2O_4$ phase, which had a higher crystallinity.

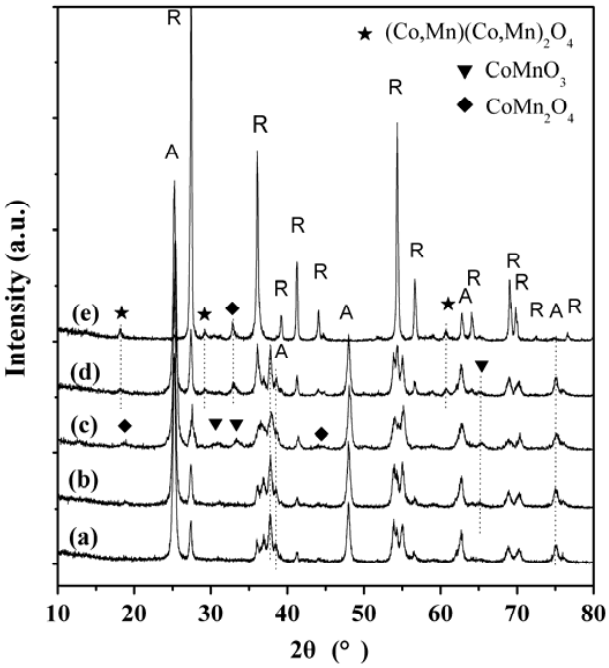

Figure 4. XRD patterns of the 10Mn-5Co/TiO_2 catalysts calcined at various temperatures: (**a**) 573 K; (**b**) 673 K; (**c**) 773 K; (**d**) 873 K; and (**e**) 973 K. (A = anatase phase of TiO_2, R = rutile phase of TiO_2).

2.4. TEM Characterization

Figure 5 shows the TEM images of 10Mn-5Co/TiO_2 calcined at 673 and 773 K. For Mn-Co/TiO_2 (673 K) in Figure 5A, the lattice fringes a and b were determined to be 0.36 and 0.45 nm, matched $CoMnO_3$ (012) (standard value is 0.362 nm) and (003) (standard value is 0.457 nm) crystal faces, respectively. For Mn-Co/TiO_2 (773 K) in Figure 5B, the lattice fringe c was determined to be 0.48 nm, corresponding to $CoMn_2O_4$ (standard value is 0.485 nm). The lattice fringes d and e were determined to be 0.35 and 0.52 nm, corresponding to anatase (101) of TiO_2 and MnO_2 (200) (standard value is 0.515 nm) crystal faces, respectively. The lattice fringes f and g were determined to be 0.36 and 0.41 nm, matched $CoMnO_3$ (012) and (101) (standard value is 0.408 nm) crystal faces, respectively. These results demonstrated the existence of $CoMnO_3$ and $CoMn_2O_4$ phases in Mn-Co/TiO_2 samples.

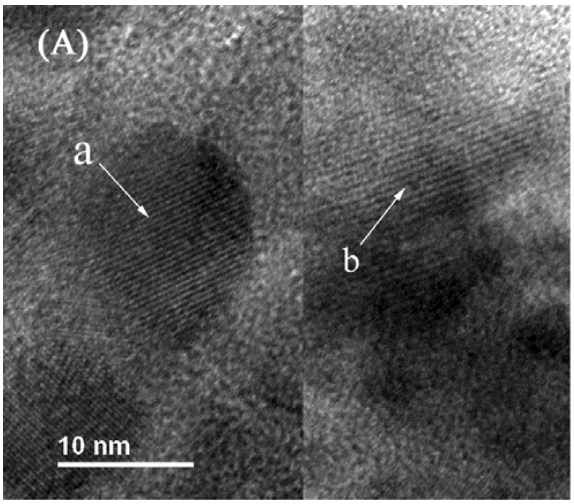

Figure 5. *Cont*.

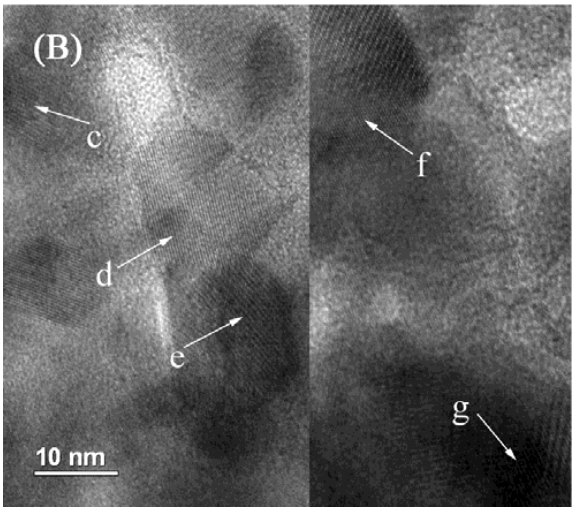

Figure 5. TEM images of the catalysts: (**A**) 10Mn-5Co/TiO_2 (673 K); and (**B**) 10Mn-5Co/TiO_2 (773 K). (a. $CoMnO_3$ (012); b. $CoMnO_3$ (003); c. $CoMn_2O_4$ (111); d. anatase (101); e. MnO_2 (200); f. $CoMnO_3$ (012); g. $CoMnO_3$ (101)).

2.5. XPS Characterization

The surface oxidation states and atomic concentrations of 10Mn/TiO_2 (773 K) and 10Mn-5Co/TiO_2 calcined at 673, 773 and 973 K were determined by XPS analysis. The photoelectron profiles of Mn 2p and O 1s are shown in Figure 6. The atomic concentrations of Mn, Co and O are listed in Table 2. To evaluate Mn valence states, a peak-fitting deconvolution was performed for these profiles fitted with a mixing of Gaussian and Lorentzian peaks after removal of a Shirley background.

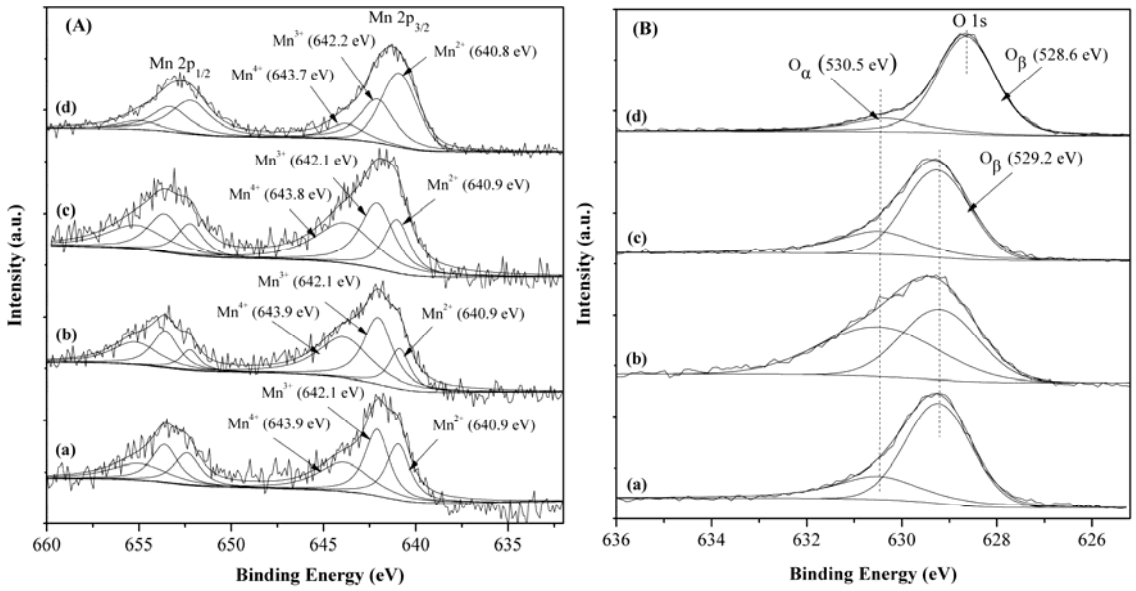

Figure 6. XPS spectra for (**A**) Mn 2p and (**B**) O 1s of the catalysts: (**a**) 10Mn/TiO_2 (773 K); (**b**) 10Mn-5Co/TiO_2 (673 K); (**c**) 10Mn-5Co/TiO_2 (773 K); and (**d**) 10Mn-5Co/TiO_2 (973 K).

In Figure 6A, two peaks were detected at 641.2–642.1 eV and 652.8–653.7 eV, belonging to Mn $2p_{3/2}$ and Mn $2p_{1/2}$, respectively. The spectra of Mn $2p_{3/2}$ could be separated into three peaks. The peaks corresponding to the higher, middle and lower binding energy were attributed to Mn^{4+}, Mn^{3+} and Mn^{2+}, respectively [25,26]. Their relative atomic ratios in the surface layer are listed in Table 2.

The increase of Mn^{4+} ratio after Co doping indicated the transformation of Mn^{2+} to Mn^{3+} and Mn^{3+} to Mn^{4+} by the addition of cobalt oxides. The reduction was resulted from the strong interaction between Mn and Co oxides. In addition, as the calcination temperature increased, the relative ratio of Mn^{4+} decreased gradually while the relative ratio of Mn^{2+} increased. The main valence state of manganese in Mn-Co/TiO_2 (673 K) was Mn^{4+}, whereas Mn^{2+} was the dominant valence state in the catalyst calcined at 973 K. It can be concluded that the Mn^{4+} oxidation state was responsible for the activity of NO oxidation at low temperatures.

Figure 6B shows the O 1s XPS spectra for these catalysts. The O 1s spectra can be separated into two peaks at around 528.6–529.2 eV and 530.5 eV. The higher binding energy one with less intensity was ascribed to adsorbed oxygen or surface hydroxyl species [27,28], referred to as O_α, whereas the lower binding energy one was due to lattice oxygen O^{2-} [28,29], denoted as O_β. The value of binding energy of O_β decreased from 529.2 to 528.6 eV when the calcination temperature increased from 773 to 973 K. The binding energies of 529.2 and 528.6 eV were attributed to the lattice oxygen of anatase TiO_2 and rutile TiO_2, respectively. The ratios of O_α:O_β in Table 2 showed an increase in chemical adsorbed oxygen by doping of Co oxides. The reason is that as a nonstoichiometric compound-like, Co oxides can adsorb and exchange oxygen easily in several surface layers [15,30], and then promote oxygen adsorption. In addition, it was found out that the relative ratio of O_α reduced from 54% to 17% when calcination temperature increased from 673 K to 973 K, indicating the inhibition for adsorption of oxygen after high-temperature calcination. The XPS results indicated that the decline of NO oxidation efficiency was related to the decrease of chemical adsorbed oxygen. Wu *et al.* [31] have suggested that chemisorbed oxygen was helpful to the oxidation of NO to NO_2.

Table 2. Surface atomic concentrations and ratios for the catalysts determined by XPS spectra.

Catalyst	Mn^{4+}:Mn^{3+}:Mn^{2+}	O_α:O_β	Mn at. %	Co at. %
10Mn/TiO_2 (773 K)	34:36:30	30:70	6.48	-
10Mn-5Co/TiO_2 (673 K)	43:39:17	54:46	5.47	2.32
10Mn-5Co/TiO_2 (773 K)	40:37:23	32:68	6.19	3.73
10Mn-5Co/TiO_2 (973 K)	14:36:50	17:83	6.73	1.54

2.6. H_2-TPR Characterization

Figure 7 presents the H_2-TPR profiles of the Mn-Co/TiO_2 catalysts with various Co contents and calcined at 773 K. The reduction profile of 5Co/TiO_2 was also provided to identify the peaks of Co oxides (Figure 7a). The profile of 5Co/TiO_2 was characterized by two reduction peaks at 693 and 824 K, due to reduction of Co_3O_4 to CoO and CoO to Co°, respectively [32]. In terms of 10Mn/TiO_2 (Figure 7b), two separate reduction peaks were observed. According to the literature [33], the lower temperature one at 670 K (T_1) could be ascribed to the reduction of MnO_2 to Mn_2O_3. The higher temperature peak could be separated to two peaks at 763 and 796 K, corresponding to the reduction of Mn_2O_3 to Mn_3O_4 and Mn_3O_4 to MnO, respectively [33]. The prominent peak at 670 K indicated that MnO_2 was present in Mn/TiO_2.

For the Mn-Co/TiO_2 catalysts with various Co contents (Figure 7c–f), it can be seen that after the addition of Co oxides into Mn/TiO_2, the profiles of the first and second peaks were similar to the reduction peaks of Mn/TiO_2. These two peaks became more and more narrow and their intensities increased with increasing Co content. Meanwhile, the summits shifted toward low temperature with the increase of Co content. As can be seen, after 10 wt. % Co was added into the catalyst, the first peak at 625 K was lower for about 45 K than the first reduction peak of Mn/TiO_2, and lower for about 68 K than that of Co/TiO_2. Consequently, it can be deduced that an interaction existed between Mn and Co oxides, leading to the down-shift of the reduction temperature and related to the higher NO oxidation

efficiency at low temperatures for Mn-Co/TiO_2. Combining with the XPS results, the interaction between Mn and Co ions can be represented as reaction (1):

$$Mn^{3+} + Co^{3+} \rightarrow Mn^{4+} + Co^{2+} \quad (1)$$

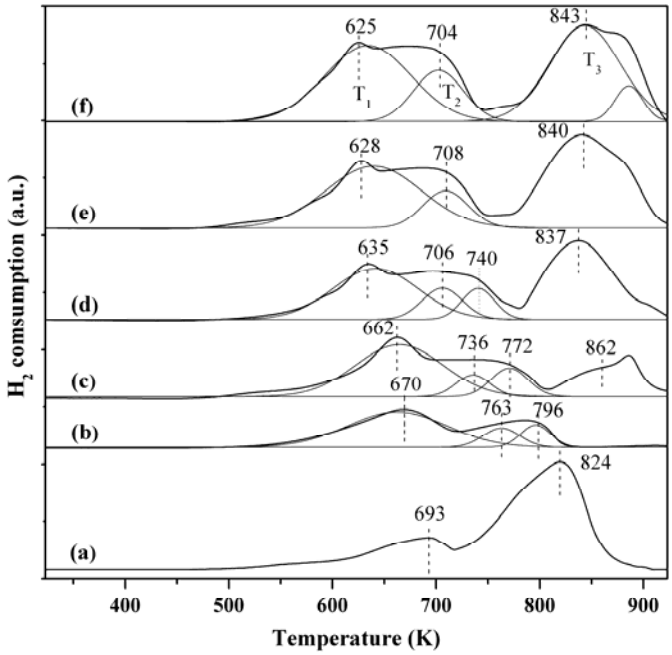

Figure 7. H_2-TPR profiles of the catalysts Mn-Co/TiO_2 (773 K) with various Co contents: (**a**) 5Co/TiO_2; (**b**) 10Mn/TiO_2; (**c**) 10Mn-2Co/TiO_2; (**d**) 10Mn-5Co/TiO_2; (**e**) 10Mn-8Co/TiO_2; and (**f**) 10Mn-10Co/TiO_2.

It is known that the Co^{3+} probably corresponds to [$Co^{2+}Co^{3+}{}_2O_4$] with a normal spinel structure [30]. Based on XRD and TEM results, $CoMnO_3$ is the main physical phase on Mn-Co/TiO_2 (773 K). From the perspective of standard electrode potential, the standard electrode potential of $Co^{3+} \rightarrow Co^{2+}$ is higher than that of $Mn^{4+} \rightarrow Mn^{3+}$ [34], and the lower the standard electrode potential, the more easily the coordinated oxygen is obtained. Apparently, if the oxygen vacancy exists in the mixed oxide of Co_3O_4 and $CoMnO_3$, the oxygen ion will preferentially coordinate to Mn^{4+} ion rather than Co^{3+} ion, which will lead to oxygen vacancy of Co_3O_4. Meanwhile, Co_3O_4 adsorbs oxygen easily on Co-contained surface and exchange with the oxygen on several surface atom layers to form $Co_3O_{4+y}{\cdot}CoMnO_3$ [15,30]. These oxygen ions are highly active and reduced easily, leading to the shift of the reduction peak toward lower temperatures compared with the Co/TiO_2. Consequently, Co doping into Mn/TiO_2 can lower the reduction temperature. When the y is small, we write $Co_3O_{4+y}{\cdot}CoMnO_3$ as $Co_3O_4{\cdot}CoMnO_3$. Therefore, the first peak of Mn-Co/TiO_2 could be ascribed to the reduction of the compound $Co_3O_4{\cdot}CoMnO_3$. The second and third reduction peak temperatures were also lower than those of Mn/TiO_2 in the similar way. Combining with XRD and XPS results, the second peak could be ascribed to the reduction of the composite oxide $CoMn_2O_4$ and the third peak could be ascribed to the reduction that the final product was $CoO{\cdot}MnO$. These two peaks trended to combination with increasing Co content, probably due to the strong oxygen adsorption ability of Co oxides. Consequently, the Mn^{3+} ions were easy to be directly reduced to Mn^{2+}. The fourth peak was due to the reduction of Co^{2+} to Co°. It shifted toward higher temperature after co-doping of Mn oxides. The Mn^{3+} ions are much reducible than the Co^{2+} ions and request lower activation energy for reduction. Accordingly, the Co^{2+} can be reduced only until the Mn^{3+} ions were reduced completely.

Figure 8 shows the H_2-TPR profiles of 10Mn-5Co/TiO_2 catalysts calcined at various temperatures. The catalysts calcined at 573 and 673 K clearly showed similar reduction peaks. The T_1 and T_2 peaks were mainly due to the reduction of Co_3O_4·$CoMnO_3$ and $CoMn_2O_4$, respectively. The intensities of the two peaks decreased gradually and the peaks broadened with the increase of calcination temperature. It indicated that the Mn-O-Co mixed oxides formation and the oxygen mobility of Mn-O-Co were affected by the calcination temperature. The TPR results were associated with the NO oxidation ability in Figure 2. For the Mn-Co/TiO_2 calcined at 573 and 673 K, the H_2 reduction peaks of T_1 corresponded to their NO oxidation peaks at 443 K. This also demonstrated that the formation of highly dispersed Co_3O_4·$CoMnO_3$ through synergistic interaction between Mn-O and Co-O was responsible for the enhanced activities towards NO oxidation. The high calcination temperature leads to catalyst sintering, difficulty in oxygen mobility of Mn-O-Co, the reduction of Mn^{4+} to Mn^{3+} and Mn^{2+}, and the transformation of $CoMnO_3$ to $(Co,Mn)(Co,Mn)_2O_4$. These factors are responsible for the decrease of NO oxidation efficiency.

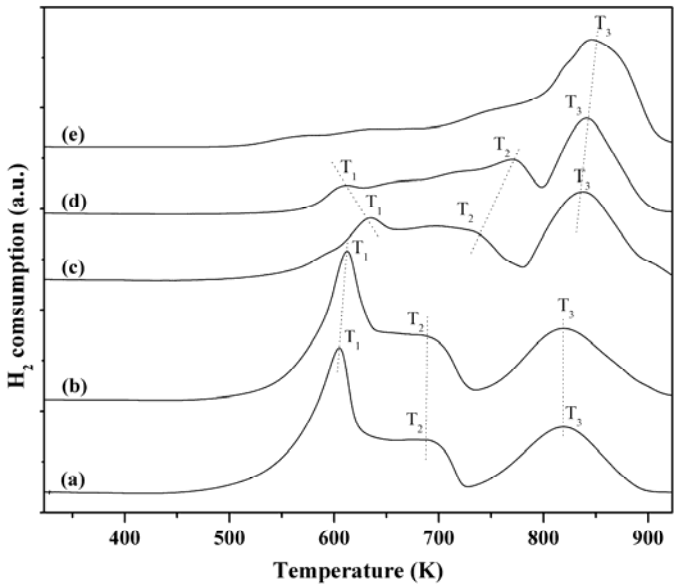

Figure 8. H_2-TPR profiles of 10Mn-5Co/TiO_2 catalysts calcined at various temperatures: (**a**) 573 K; (**b**) 673 K; (**c**) 773 K; (**d**) 873 K; and (**e**) 973 K.

3. Experimental Section

3.1. Catalyst Preparation

The catalysts were prepared by wet impregnating method using TiO_2 P25 (99.5%, Evonic Degussa, Germany) as support materials. $Mn(NO_3)_2$ solution (50.0%, Damao, Tianjing, China) and $Co(NO_3)_3 \cdot 6H_2O$ (99.0%, Damao, Tianjing, China) were used as the precursors. The required amounts of precursors were dissolved into 5 mL deionized water and then 6.0 g of support was added into the solution. The mixed solution was stirred for 1 h and left at room temperature for 24 h. Subsequently, the samples were dried at 383 K for 12 h, followed by calcination in air for 3 h at 573–973 K. The manganese loadings were selected as 10 wt. %, and the cobalt contents were varied ranging from 0 to 10 wt. %. The catalysts were simply denoted as *x*Mn-*y*Co/TiO_2 (T), where *x* and *y* represented the weight percentages of Mn and Co to TiO_2, respectively, and T represented the calcination temperature.

3.2. Catalyst Evaluation

The catalytic activity tests were carried out in a fixed bed quartz reactor (i.d. 8 mm) containing 0.15 g of the catalyst (60–100 mesh). The simulated gas mixture (contained 400 ppm NO, 5 vol. %

O_2 and Ar balance) was fed to the reactor with a gas hourly space velocity (GHSV) of 42,000 h^{-1}. The reaction temperature was increased from 373 to 593 K at a heating rate of 1 K/min. The reactor temperature was controlled by a thermocouple and a PID-regulation system (CKW-2200, Bachy, Beijing, China). The outlet gas was monitored using an online nitrogen oxides analyzer (EC9841B, Ecotech, Ferntree Gully, Australia) to test the concentrations of NO, NO_2 and NO_x.

The percentage of NO oxidation to NO_2 was calculated as Equation (2):

$$[\text{Conv.}]_{\text{NO}} = ([\text{NO}]_{in} - [\text{NO}]_{out})/[\text{NO}]_{in} \times 100\% \quad (2)$$

3.3. Catalyst Characterization

Specific surface area and pore size distribution of the samples were measured using a BELSORP-mini II instrument (Ankersmid, Holland), through nitrogen adsorption at liquid nitrogen temperature (77 K) after degassing samples in vacuum at 573 K for 3 h.

The crystalline phases of the catalysts were determined by X-ray diffractometer (RIGAKU, D/Max 2500PC, Tokyo, Japan) in the 2θ angle range of 10–80° using Cu Kα radiation combined with nickel filter.

Detailed physical structural characteristics were observed with a transmission electron microscope (Tecnai G^2 F30, FEI, Hillsboro, OR, USA). Samples were prepared by ultrasonic dispersion in ethanol. The suspension was deposited on a Lacey-carbon film (Beijing, China), which was supported on a copper grid.

The surface oxidation states and atomic concentrations of samples were analyzed by a X-ray photoelectron spectrometer (ULVAC-PHI 1800, Tokyo, Japan) using Al Kα as a radiation source. The binding energy of the C 1s peak at 284.6 eV was taken for correcting the obtained spectra.

The H_2-Temperature programmed reduction experiments were carried out with 0.05 g catalysts under a total flow rate of 40 mL/min. Before the TPR measurements, the catalysts were pretreated in a flow of N_2 at 573 K for 1 h and subsequently cooled to 323 K. Then the TPR runs were carried out from 323 to 923 K with a flow of 5% H_2/N_2 at a heating rate of 10 K/min. The consumption of H_2 was continuously monitored using an online gas chromatograph (GC 6890, Qingdao, China) with a thermal conductivity detector (TCD).

4. Conclusions

A series of Mn-Co/TiO_2 catalysts were prepared by wet impregnation method and developed for the catalytic oxidation of NO to NO_2 below 593 K. The bimetallic catalysts Mn-Co/TiO_2 showed higher catalytic abilities than the Mn/TiO_2 and Co/TiO_2 within the temperature range of 403–473 K. The Mn-Co/TiO_2 calcined at 573 and 673 K showed excellent activities for NO oxidation at low temperatures. The correlations among the catalytic performances and the redox properties of the catalysts were investigated. It was found from the XRD, TEM and H_2-TPR results that the $CoMnO_3$ mixed oxides were formed, which led to the shift of the reduction peak toward low temperatures. The XPS results revealed the increase of chemical adsorbed oxygen and Mn^{4+} ratio by doping Co into Mn/TiO_2. Increasing calcination temperature led to the decrease of chemical adsorbed oxygen amounts and the reduction of Mn^{4+} to Mn^{3+} and Mn^{2+}. In conclusion, the higher the amount of chemically adsorbed oxygen, the higher the amount of Mn^{4+} ions, and the formation of dispersed $Co_3O_4{\cdot}CoMnO_3$ mixed oxides were helpful to the oxidation of NO to NO_2 at low temperatures.

Acknowledgments: This project was financially supported by Foundation Science and Technology innovation Committee of Shenzhen, China (No. JCYJ20140417172417138 and No. ZDSYS20140508161622508).

Author Contributions: Feng Ouyang, Lu Qiu, and Yun Wang contributed to the experimental design. Lu Qiu, Yun Wang and Changliang Zhang contributed to all the experimental data collection. Lu Qiu wrote the first draft of the manuscript, which was then extensively improved by Feng Ouyang, Dandan Pang and Gang Cao.

Conflicts of Interest: The authors declare no conflict of interest.

References

1. Epling, W.S.; Campbell, L.E.; Yezerets, A.; Currier, N.W.; Parks, J.E. Overview of the Fundamental Reactions and Degradation Mechanisms of NO_x Storage/Reduction Catalysts. *Catal. Rev. Sci. Eng.* **2004**, *46*, 163–245.
2. Nova, I.; Ciardelli, C.; Tronconi, E.; Chatterjee, D.; Bandl-Konrad, B. NH_3-NO/NO_2 chemistry over V-based catalysts and its role in the mechanism of the Fast SCR reaction. *Catal. Today* **2006**, *114*, 3–12. [CrossRef]
3. Amberntsson, A.; Fridell, E.; Skoglundh, M. Influence of platinum and rhodium composition on the NO_x storage and sulphur tolerance of a barium based NO_x storage catalyst. *Appl. Catal. B* **2003**, *46*, 429–439. [CrossRef]
4. Li, L.; Qu, L.; Cheng, J.; Li, J.; Hao, Z. Oxidation of nitric oxide to nitrogen dioxide over Ru catalysts. *Appl. Catal. B* **2009**, *88*, 224–231. [CrossRef]
5. Salasc, S.; Skoglundh, M.; Fridell, E. A comparison between Pt and Pd in NO_x storage catalysts. *Appl. Catal. B* **2002**, *36*, 145–160. [CrossRef]
6. Weiss, B.M.; Iglesia, E. Mechanism and site requirements for NO oxidation on Pd catalysts. *J. Catal.* **2010**, *272*, 74–81. [CrossRef]
7. Guillén-Hurtado, N.; Atribak, I.; Bueno-López, A.; García-García, A. Influence of the cerium precursor on the physico-chemical features and NO to NO_2 oxidation activity of ceria and ceria-zirconia catalysts. *J. Mol. Catal. A* **2010**, *323*, 52–58. [CrossRef]
8. Metkar, P.S.; Balakotaiah, V.; Harold, M.P. Experimental and kinetic modeling study of NO oxidation: Comparison of Fe and Cu-zeolite catalysts. *Catal. Today* **2012**, *184*, 115–128. [CrossRef]
9. Vijay, R.; Hendershot, R.J.; Rivera-Jiménez, S.M.; Rogers, W.B.; Feist, B.J.; Snively, C.M.; Lauterbach, J. Noble metal free NO_x storage catalysts using cobalt discovered via high-throughput experimentation. *Catal. Commun.* **2005**, *6*, 167–171. [CrossRef]
10. Wang, H.; Wang, J.; Wu, Z.; Liu, Y. NO Catalytic Oxidation Behaviors over CoO_x/TiO_2 Catalysts Synthesized by Sol-Gel Method. *Catal. Lett.* **2010**, *134*, 295–302. [CrossRef]
11. Wu, Z.; Tang, N.; Xiao, L.; Liu, Y.; Wang, H. MnO_x/TiO_2 composite nanoxides synthesized by deposition-precipitation method as a superior catalyst for NO oxidation. *J. Colloid Interface Sci.* **2010**, *352*, 143–148. [CrossRef] [PubMed]
12. Brik, Y.; Kacimi, M.; Ziyad, M.; Bozon-Verduraz, F. Titania-Supported Cobalt and Cobalt-Phosphorus Catalysts: Characterization and Performances in Ethane Oxidative Dehydrogenation. *J. Catal.* **2001**, *202*, 118–128. [CrossRef]
13. Yang, W.-H.; Kim, M.H.; Ham, S.-W. Effect of calcination temperature on the low-temperature oxidation of CO over CoO_x/TiO_2 catalysts. *Catal. Today* **2007**, *123*, 94–103. [CrossRef]
14. Zafeiratos, S.; Dintzer, T.; Teschner, D.; Blume, R.; Hävecker, M.; Knop-Gericke, A.; Schlögl, R. Methanol oxidation over model cobalt catalysts: Influence of the cobalt oxidation state on the reactivity. *J. Catal.* **2010**, *269*, 309–317. [CrossRef]
15. Petitto, S.C.; Marsh, E.M.; Carson, G.A.; Langell, M.A. Cobalt oxide surface chemistry: The interaction of CoO(100), Co_3O_4(110) and Co_3O_4(111) with oxygen and water. *J. Mol. Catal. A* **2008**, *281*, 49–58. [CrossRef]
16. Irfan, M.F.; Goo, J.H.; Kim, S.D. Co_3O_4 based catalysts for NO oxidation and NO_x reduction in fast SCR process. *Appl. Catal. B* **2008**, *78*, 267–274. [CrossRef]
17. Ettireddy, P.R.; Ettireddy, N.; Boningari, T.; Pardemann, R.; Smirniotis, P.G. Investigation of the selective catalytic reduction of nitric oxide with ammonia over Mn/TiO_2 catalysts through transient isotopic labeling and *in situ* FT-IR studies. *J. Catal.* **2012**, *292*, 53–63. [CrossRef]
18. Boningari, T.; Pappas, D.K.; Ettireddy, P.R.; Kotrba, A.; Smirniotis, P.G. Influence of SiO_2 on M/TiO_2 (M = Cu, Mn, and Ce) formulations for low-temperature selective catalytic reduction of NO_x with NH_3: Surface properties and key components in relation to the activity of NO_x reduction. *Ind. Eng. Chem. Res.* **2015**, *54*, 2261–2273. [CrossRef]
19. Thirupathi, B.; Smirniotis, P.G. Co-doping a metal (Cr, Fe, Co, Ni, Cu, Zn, Ce, and Zr) on Mn/TiO_2 catalyst and its effect on the selective reduction of NO with NH_3 at low-temperatures. *Appl. Catal. B* **2011**, *110*, 195–206. [CrossRef]
20. Liu, Z.; Yi, Y.; Zhang, S.; Zhu, T.; Zhu, J.; Wang, J. Selective catalytic reduction of NO_x with NH_3 over Mn-Ce mixed oxide catalyst at low temperatures. *Catal. Today* **2013**, *216*, 76–81. [CrossRef]

21. Yu, J.; Guo, F.; Wang, Y.; Zhu, J.; Liu, Y.; Su, F.; Gao, S.; Xu, G. Sulfur poisoning resistant mesoporous Mn-base catalyst for low-temperature SCR of NO with NH_3. *Appl. Catal. B* **2010**, *95*, 160–168. [CrossRef]
22. Lee, S.M.; Park, K.H.; Kim, S.S.; Kwon, D.W.; Hong, S.C. Effect of the Mn oxidation state and lattice oxygen in Mn-based TiO_2 catalysts on the low-temperature selective catalytic reduction of NO by NH_3. *J. Air Waste Manag.* **2012**, *62*, 1085–1092. [CrossRef]
23. Qi, G.; Yang, R.T. Low-temperature selective catalytic reduction of NO with NH_3 over iron and manganese oxides supported on titania. *Appl. Catal. B* **2003**, *44*, 217–225. [CrossRef]
24. Meng, B.; Zhao, Z.; Chen, Y.; Wang, X.; Li, Y.; Qiu, J. Low-temperature synthesis of Mn-based mixed metal oxides with novel fluffy structures as efficient catalysts for selective reduction of nitrogen oxides by ammonia. *Chem. Commun.* **2014**, *50*, 12396–12399. [CrossRef] [PubMed]
25. Venkataswamy, P.; Jampaiah, D.; Lin, F.; Alxneit, I.; Reddy, B.M. Structural properties of alumina supported Ce-Mn solid solutions and their markedly enhanced catalytic activity for CO oxidation. *Appl. Surf. Sci.* **2015**, *349*, 299–309. [CrossRef]
26. Yao, Y.; Cai, Y.; Wu, G.; Wei, F.; Li, X.; Chen, H.; Wang, S. Sulfate radicals induced from peroxymonosulfate by cobalt manganese oxides $Co_xMn_{3-x}O_4$ for Fenton-Like reaction in water. *J. Hazard. Mater.* **2015**, *296*, 128–137. [CrossRef] [PubMed]
27. Rida, K.; Benabbas, A.; Bouremmad, F.; Peña, M.A.; Martínez-Arias, A. Surface properties and catalytic performance of $La_{1-x}Sr_xCrO_3$ perovskite-type oxides for CO and C_3H_6 combustion. *Catal. Commun.* **2006**, *7*, 963–968. [CrossRef]
28. Sutthiumporn, K.; Kawi, S. Promotional effect of alkaline earth over Ni-La_2O_3 catalyst for CO_2 reforming of CH_4: Role of surface oxygen species on H_2 production and carbon suppression. *Int. J. Hydrog. Energ.* **2011**, *36*, 14435–14446. [CrossRef]
29. Merino, N.A.; Barbero, B.P.; Eloy, P.; Cadús, L.E. $La_{1-x}Ca_xCoO_3$ perovskite-type oxides: Identification of the surface oxygen species by XPS. *Appl. Surf. Sci.* **2006**, *253*, 1489–1493. [CrossRef]
30. Petitto, S.C.; Langell, M.A. Surface composition and structure of Co_3O_4(110) and the effect of impurity segregation. *J. Vac. Sci. Technol. A* **2004**, *22*, 1690–1696. [CrossRef]
31. Wu, Z.; Jin, R.; Liu, Y.; Wang, H. Ceria modified MnO_x/TiO_2 as a superior catalyst for NO reduction with NH_3 at low-temperature. *Catal. Commun.* **2008**, *9*, 2217–2220. [CrossRef]
32. Wang, Z.L.; Yin, J.S.; Mo, W.D.; Zhang, Z.J. *In-Situ* Analysis of Valence Conversion in Transition Metal Oxides Using Electron Energy-Loss Spectroscopy. *J. Phys. Chem. B* **1997**, *101*, 6794–6798. [CrossRef]
33. Sreekanth, P.M.; Pena, D.A.; Smirniotis, P.G. Titania Supported Bimetallic Transition Metal Oxides for low-temperature SCR of NO with NH_3. *Ind. Eng. Chem. Res.* **2006**, *45*, 6444–6449. [CrossRef]
34. Standard Electrode Potential (Data Page). Available online: https://en.wikipedia.org/wiki/Standard_electrode_potential_(data_page) (accessed on 19 October 2015).